Scientific Research Publishing

Advances in Materials Physics and Chemistry, 2017, 7, 1-10
http://www.scirp.org/journal/ampc
ISSN Online: 2162-5328
ISSN Print: 2162-531X

Arsenic and Chlorine Co-Doping to $CH_3NH_3PbI_3$ Perovskite Solar Cells

Tsuyoshi Hamatani, Yasuhiro Shirahata, Yuya Ohishi, Misaki Fukaya, Takeo Oku*

Department of Materials Science, The University of Shiga Prefecture, Hikone, Japan
Email: *oku@mat.usp.ac.jp

How to cite this paper: Hamatani, T., Shirahata, Y., Ohishi, Y., Fukaya, M. and Oku, T. (2017) Arsenic and Chlorine Co-Doping to $CH_3NH_3PbI_3$ Perovskite Solar Cells. *Advances in Materials Physics and Chemistry*, **7**, 1-10.
http://dx.doi.org/10.4236/ampc.2017.71001

Received: October 6, 2016
Accepted: January 8, 2017
Published: January 11, 2017

Abstract

Arsenic (As) and chlorine (Cl) were co-doped to $CH_3NH_3PbI_3$ perovskite solar cells, and the photovoltaic properties were investigated. AsI_3 and NH_4Cl were added to perovskite precursor solution, which were deposited on mesoporous TiO_2 by a spin-coating combining an air flow method. Current density-voltage characteristics and incident photon-to-current conversion efficiencies were improved by the co-doping of As and Cl to the perovskite phase, which also indicated an energy gap of 1.57 eV. X-ray diffraction showed suppression of PbI_2 formation by the AsI_3 addition. The structure analysis by scanning electron microscopy indicated formation of a homogeneous microstructure by adding AsI_3 with NH_4Cl, which would result in the improvement of the photovoltaic properties.

Keywords

Perovskite, Arsenic, Solar Cell, NH_4Cl, Chlorine

1. Introduction

Since the discovery of application of $CH_3NH_3PbI_3$ compounds to solar cells [1], various types of solar cells have been fabricated and characterized [2] [3] [4] [5]. To improve the photovoltaic properties, halogen doping, such as chlorine (Cl) or bromine (Br) at the iodine (I) sites of the $CH_3NH_3PbI_3$ has been studied [6] [7] [8]. The doped Cl would lengthen the diffusion length of excitons, which resulted in the improvement of the efficiency [9] [10].

Additionally, studies on elemental doping such as tin (Sn) [11], antimony (Sb) [12] [13], germanium (Ge) [14] [15], thallium (Tl) [15], or indium (In) [15] at the lead (Pb) sites have been carried out. Especially, the conversion efficiencies were improved by Sb-doping to the perovskite phase [12] [13]. To improve the photovoltaic properties, detailed searches on the metal and halogen doping at the Pb and I sites are needed.

The purpose of the present work is to investigate a co-doping effect of arsenic (As) and Cl to $CH_3NH_3PbI_3$ perovskite solar cells. As a group 15 element, it would be expected to improve the photovoltaic properties as previously reported Sb doping to the $CH_3NH_3PbI_3$ [12] [14]. Cl is expected to increase the carrier diffusion length in the perovskite phase [9] [10], and an improvement of the morphology of the perovskite films is also expected by adding NH_4Cl [16] [17]. Devices were fabricated by a spin-coating, and the photovoltaic properties and microstructures were investigated by light-induced current density-voltage (*J-V*) characteristics, incident photon-to-current conversion efficiency (IPCE), scanning electron microscopy (SEM) with energy dispersive X-ray spectrometry (EDS), and X-ray diffraction (XRD).

2. Experimental Procedure

A schematic illustration of the fabrication process of the present TiO_2/$CH_3NH_3Pb(As)I_3(Cl)$ photovoltaic cells is shown in Figure 1. The details of the fabrication process are described in the reported papers [2] [12] [13], except for AsI_3 addition. F-doped tin oxide (FTO) substrates were cleaned using an ultrasonic bath with acetone and methanol, and dried under nitrogen gas. 0.15 M and 0.30 M TiO_2 precursor solution was prepared from titanium diisopropoxide bis(acetylacetonate) (Sigma-Aldrich, Tokyo, Japan, 0.055 mL and 0.11 mL) with 1-butanol (1 mL), and the 0.15 M TiO_2 precursor solution was casted on the FTO substrate at 3000 rpm for 30 s, and heated at 125˚C for 5 min. Then, the 0.30 M TiO_2 precursor solution was casted on the TiO_x layer at 3000 rpm for 30 s, and heated at 125˚C for 5 min. This casting process of 0.30 M solution was performed two times, and the TiO_x was sintered at 500˚C for 30 min to form the compact TiO_2 layer. After that, a mesoporous TiO_2 layer was formed on the compact TiO_2 layer by spin-coating at 5000 rpm for 30 s. For the mesoporous TiO_2 layer, the TiO_2 paste was prepared with TiO_2 powder (Nippon Aerosil, Tokyo, Japan, P-25) with poly (ethylene glycol) (Nacalai Tesque, Kyoto, Japan,

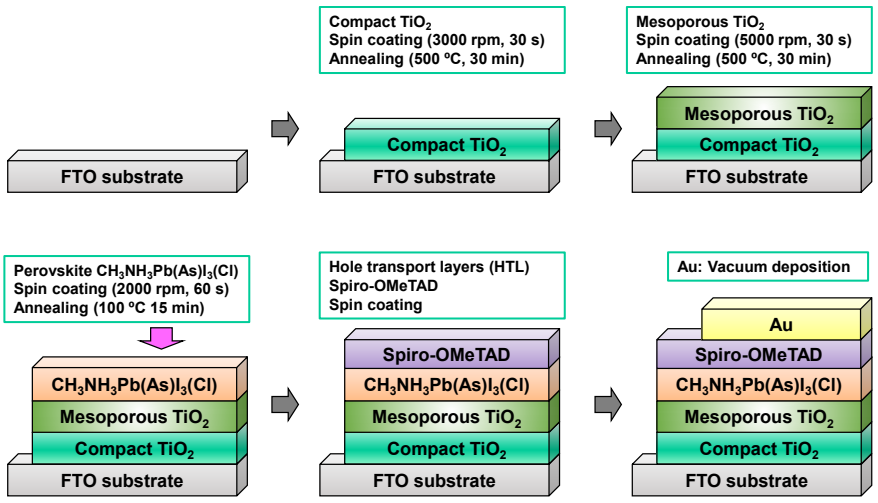

Figure 1. Schematic illustration for the fabrication of $CH_3NH_3Pb(As)I_3(Cl)$ photovoltaic cells.

PEG #20000) in ultrapure water. The solution was mixed with acetylacetone (Wako Pure Chemical Industries, Osaka, Japan, 10 μL) and triton X-100 (Sigma-Aldrich, Tokyo, Japan, 5 μL) for 30 min, and was left for 12 h to suppress the bubbles in the solution. The cells were annealed at 120˚C for 5 min and at 500˚C for 30 min to form the mesoporous TiO_2 layer. A solution of CH_3NH_3I (Showa Chemical Co., Ltd., Tokyo, Japan, 98.8 mg), PbI_2 (Sigma-Aldrich, Tokyo, Japan), NH_4Cl (Wako Pure Chemicals Industries, Ltd., Osaka, Japan), and AsI_3 (Sigma-Aldrich) with a desired mole ratio in γ-butyrolactone (Nacalai Tesque, 350 μL) and N,N-dimethylformamide (DMF, Sigma-Aldrich, 150 μL), was mixed at 60˚C. DMF and NH_4Cl were added to γ-butyrolactone to improve photovoltaic properties [13] [16] [17] [18]. The detailed preparation compositions of $TiO_2/CH_3NH_3Pb(As)I_3(Cl)$ cells with different additives are listed in **Table 1**. The solution of $CH_3NH_3Pb(As)I_3(Cl)$ was then introduced into the TiO_2 mesopores by a spin-coating and an air flow method at 50˚C, and annealed at 100˚C for 15 min. Then, a hole transport layer (HTL) was prepared by spin-coating. As the HTL, a solution of 2,2',7,7'-tetrakis [N, Ndi (p-methoxyphenyl) amino]-9,9'-spirobifluorene (spiro-OMeTAD, Wako Pure Chemical Industries, 36.1 mg) in chlorobenzene (Wako Pure Chemical Industries, 0.5 mL) was mixed with a solution of lithium bis (trifluoromethylsulfonyl) imide (Li-TFSI, Tokyo Chemical Industry, Tokyo, Japan, 260 mg) in acetonitrile (Nacalai Tesque, 0.5 mL) for 12 h. The former solution with 4-tert-butylpyridine (Aldrich, 14.4 μL) was mixed with the Li-TFSI solution (8.8 μL) for 30 min at 70˚C. All procedures were carried out in air. Finally, gold (Au) metal contacts were evaporated as top electrodes. Layered structures of the present photovoltaic cells are denoted as $FTO/TiO_2/CH_3NH_3Pb(As)I_3(Cl)$/spiro-OMeTAD/Au, as shown in **Figure 1**.

The *J-V* characteristics of the photovoltaic cells were measured under illumination at 100 mW cm^{-2} by using an AM 1.5 solar simulator (San-ei Electric, Osaka, Japan, XES-301S). The solar cells were illuminated through the side of the FTO substrates, and the illuminated area was 0.090 cm^2. The IPCE of the cells were also investigated (Enli Technology, Kaohsiung, QE-R). The microstructures of the thin films were investigated by using an X-ray diffractometer (Bruker, Kanagawa, Japan, D2 PHASER) and a scanning electron microscope (Jeol, Tokyo, Japan, JSM-6010PLUS/LA) equipped with EDS.

3. Results and Discussion

The *J-V* characteristics of the $TiO_2/CH_3NH_3Pb(As)I_3(Cl)$/spiro-OMeTAD

Table 1. Preparation composition of $TiO_2/CH_3NH_3Pb_{1-x}As_xI_3Cl_{3-y}$ cells with different additives.

Preparation Composition	Amount of Additives
$CH_3NH_3PbI_3$	None
$CH_3NH_3PbI_3Cl_{0.15}$	NH_4Cl (5 mg)
$CH_3NH_3Pb_{0.95}As_{0.05}I_{3.05}$	AsI_3 (14.5 mg)
$CH_3NH_3Pb_{0.95}As_{0.05}I_{3.05}Cl_{0.15}$	AsI_3 (14.5 mg) + NH_4Cl (5 mg)

photovoltaic cells under illumination are shown in Figure 2. The measured photovoltaic parameters of $TiO_2/CH_3NH_3Pb(As)I_3(Cl)$ cells are also summarized in Table 2. The $CH_3NH_3PbI_3$ cell provided a power conversion efficiency (η) of 0.249%, and the averaged efficiency (η_{ave}) of four electrodes on the cells is 0.171%. A short-circuit current density (J_{SC}) increased up to 11.1 mA cm^{-2} by addition of AsI_3, which would imply an increase of carrier concentration. The highest efficiency was obtained for a cell added with [AsI_3 + NH_4Cl], which provided an η of 6.31%, a fill factor (FF) of 0.563, a J_{SC} of 13.9 mA cm^{-2}, and an open-circuit voltage (V_{OC}) of 0.807 V. A J_{SC} value for the AsI_3-doped sample increased further by adding NH_4Cl, as observed in Figure 2.

IPCE spectra of the $CH_3NH_3Pb(As)I_3(Cl)$ cells are shown in Figure 3. The perovskite $CH_3NH_3Pb(As)I_3(Cl)$ shows photoconversion efficiencies between 300 nm and 790 nm, which corresponds to an energy gap of 1.57 eV. The IPCE was improved in the range of 350 - 750 nm by adding As and Cl.

Figure 4(a) shows XRD patterns of $CH_3NH_3Pb(As)I_3(Cl)$ cells on the FTO/TiO_2. The observed diffraction peaks and reported values are summarized as Table 3. The diffraction peaks can be indexed by a tetragonal crystal system (*I4/mcm*), as shown in Figure 4(b). A tetragonal structure is sometimes included in the cubic perovskite phase [8] [19], and they indicates that the fabricated films are a single perovskite structure. In addition to the perovskite phase, diffraction peaks of attributed to PbI_2 appeared in the $CH_3NH_3PbI_3(Cl)$ films, as

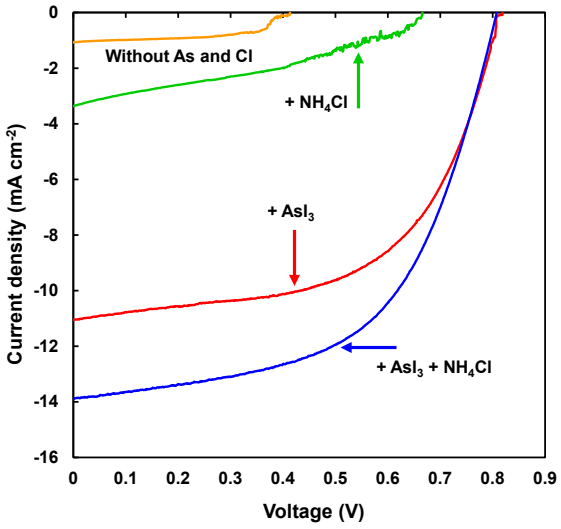

Figure 2. *J-V* characteristic of $TiO_2/CH_3NH_3Pb_{1-x}As_xI_3Cl_{3-y}$ photovoltaic cells.

Table 2. Measured photovoltaic parameters of $TiO_2/CH_3NH_3Pb_{1-x}As_xI_3Cl_{3-y}$ cells.

Additive	J_{SC} (mA cm^{-2})	V_{OC} (V)	FF	η (%)	η_{ave} (%)
None	1.07	0.414	0.562	0.249	0.171
NH_4Cl	3.36	0.665	0.360	0.805	0.415
AsI_3	11.1	0.813	0.573	5.15	3.64
AsI_3 + NH_4Cl	13.9	0.807	0.563	6.31	5.04

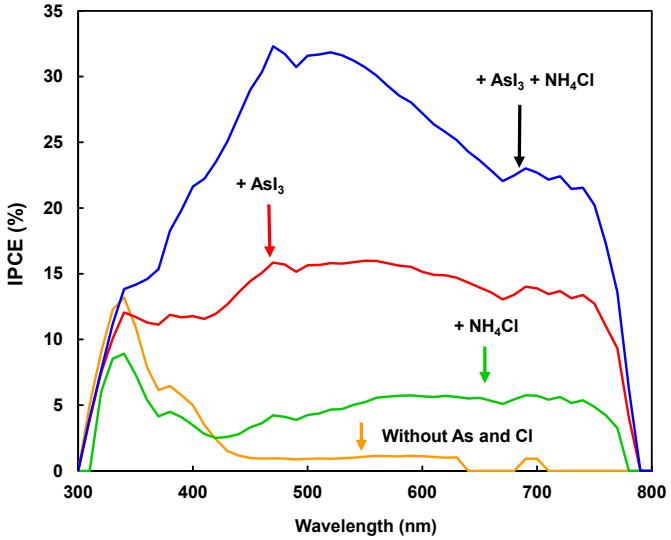

Figure 3. IPCE spectra of TiO_2/CH_3NH_3 $Pb_{1-x}As_xI_3Cl_{3-y}$ cells.

Table 3. Measured photovoltaic parameters of $TiO_2/CH_3NH_3Pb_{1-x}As_xI_3Cl_{3-y}$ cells.

		Reference data		Present work	
Material	Index	2θ (˚)	*d*-spacing (Å)	2θ (˚)	*d*-spacing (Å)
PbI_2 [20]	0 0 1	12.677	6.9770	12.69	6.973
	1 0 1	25.926	3.4339	-	-
TiO_2 [21]	1 0 1	25.271	3.5214	25.32	3.514
SnO_2 [22]	1 1 0	26.585	3.3503	26.53	3.357
	1 0 1	33.875	2.6441	33.79	2.650
$CH_3NH_3PbI_3$ [23]	0 0 2	13.951	6.3425	13.81	6.409
	1 1 0	14.222	6.2225	14.12	6.270
	2 0 0	20.165	4.4000	20.05	4.425
	2 1 1	23.651	3.7587	23.51	3.781
	2 0 2	24.604	3.6152	24.55	3.624
	2 2 0	28.668	3.1113	28.47	3.133
	3 1 0	32.139	2.7828	31.89	2.804

shown in **Figure 4(a)**, which indicates that the As addition suppressed the formation of PbI_2.

Figure 5(a) is a SEM image of $TiO_2/CH_3NH_3Pb(As)I_3$ cell with an additive of AsI_3, and the particle sizes are approximately 2 - 3 μm. Elemental mapping images of Pb, As, I, C, and N by SEM-EDX are shown in **Figure 5(b)-(f)**, respectively. The elemental mapping images indicate the particles observed in **Figure 5(a)** would correspond to the $CH_3NH_3PbI_3$ phase.

Figure 6(a) is a SEM image of $CH_3NH_3Pb(As)I_3(Cl)$ cell. By adding NH_4Cl to the $CH_3NH_3Pb(As)I_3$, the surface morphology was drastically changed, and dense packing of particles is observed. Elemental mapping images of Pb, As, I, C, N, and Cl are shown in **Figure 6(b)-(g)**, respectively. **Figure 6** indicates the

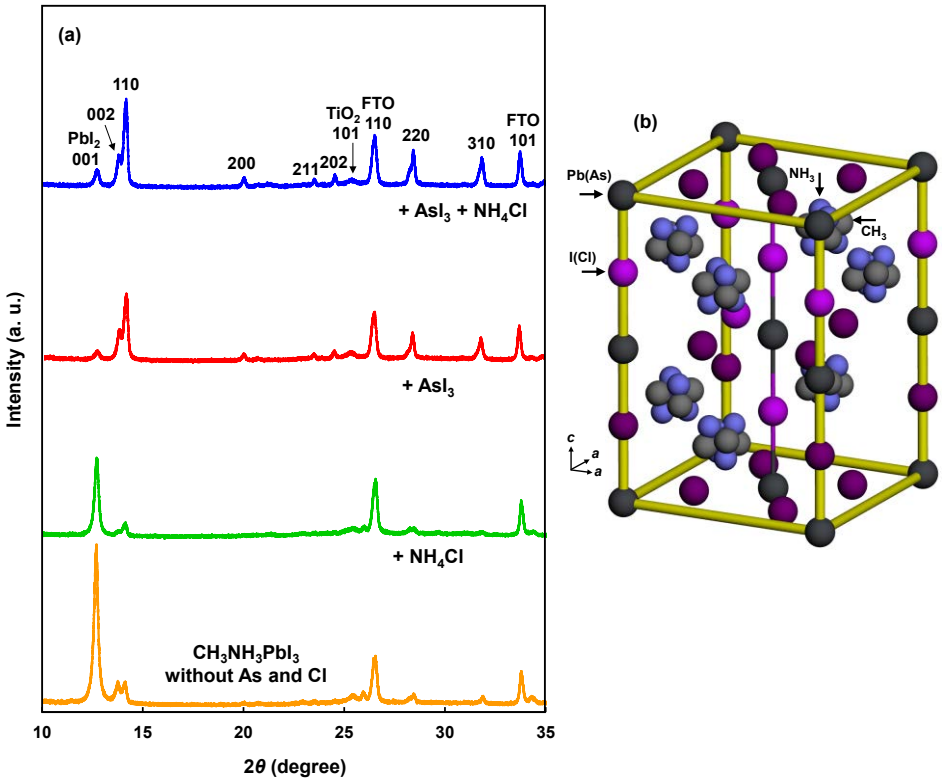

Figure 4. (a) XRD patterns of $TiO_2/CH_3NH_3Pb_{1-x}As_xI_3Cl_{3-y}$ cells. (b) Structure model of tetragonal $CH_3NH_3Pb(As)I_3(Cl)$. Indices are based on a tetragonal system.

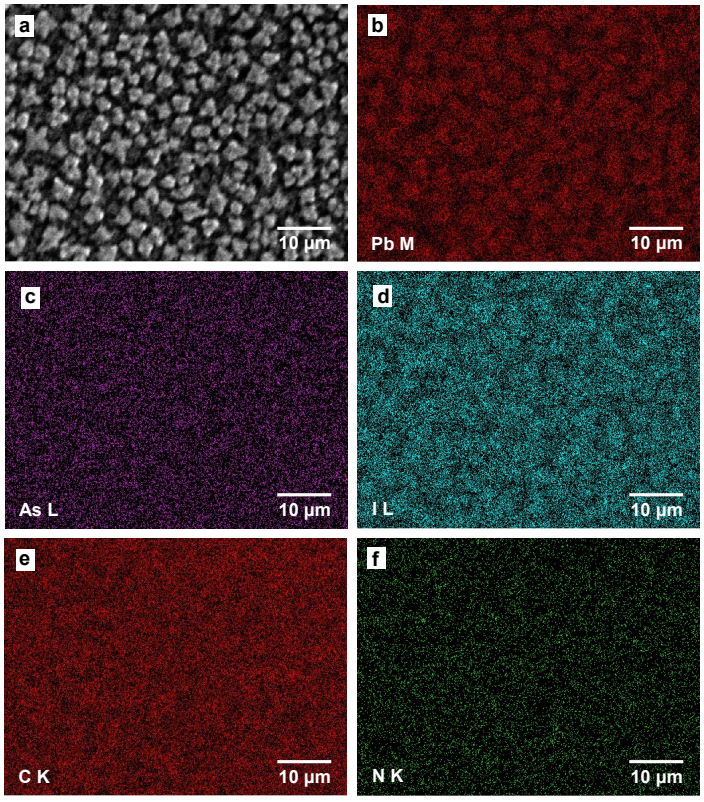

Figure 5. (a) SEM image of $CH_3NH_3Pb(As)I_3$ cell with an additive of AsI_3. Elemental mapping images of (b) Pb M line, (c) As L line, (d) I L line, (e) C K line, and (f) N K line.

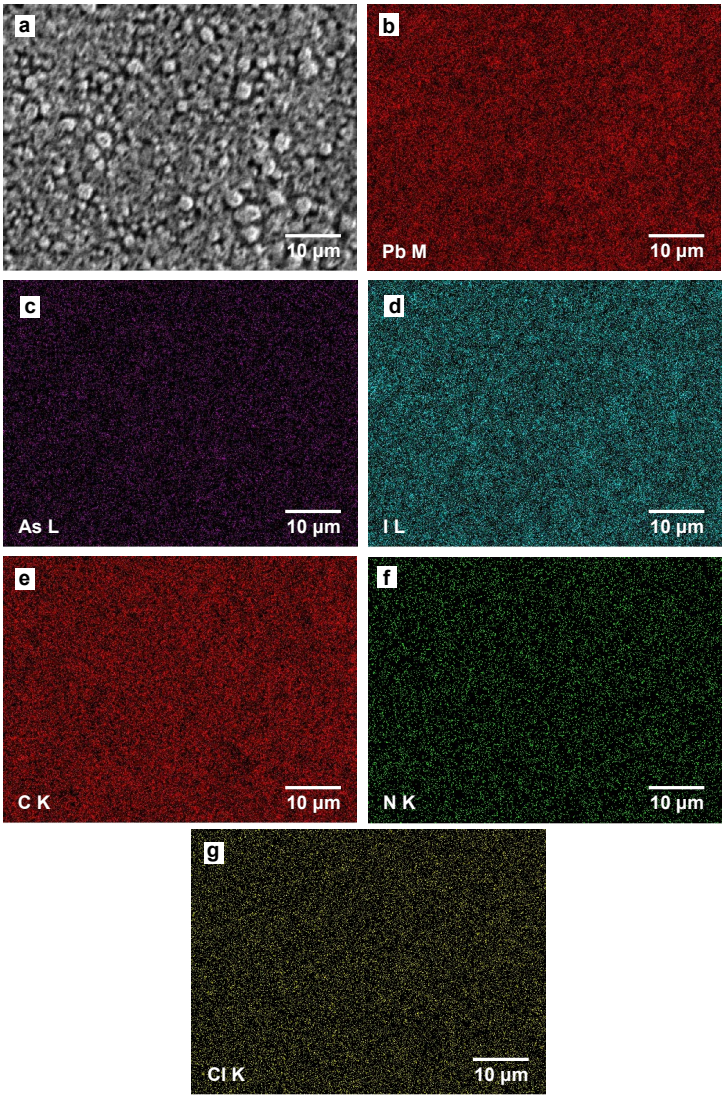

Figure 6. (a) SEM image of $CH_3NH_3Pb(As)I_3(Cl)$ cell with additives of AsI_3 with NH_4Cl. Elemental mapping images of (b) Pb M line, (c) As L line, (d) I L line, (e) C K line, (f) N K line, and (g) Cl K line.

perovskite $CH_3NH_3PbI_3$ phase is dispersed homogeneously on the device surface. Table 4 shows a composition ratio of Pb, As, I, Cl and C:N calculated from the EDX spectrum. Basic compositions were calculated only on the Pb, As, I and Cl elements, and iodine is the highest percentage in these elements. To investigate the C:N ratio in the perovskite crystal, the C:N composition ratio was also calculated separately. This result indicates that I would be deficient from the starting composition of $CH_3NH_3Pb(As)I_3(Cl)$, and the deficient I might increase the hole concentration.

An energy level diagram of $TiO_2/CH_3NH_3Pb(As)I_3(Cl)$ photovoltaic cells is proposed as shown in Figure 7. The electronic charge generation is caused by light irradiation from the bottom of FTO substrate side. The TiO_2 layer receives the electrons from the $CH_3NH_3Pb(As)I_3(Cl)$ layer, and the electrons are transported to the FTO. The holes are transported to an Au electrode through spiro-OMeTAD.

Table 4. Measured compositions of $TiO_2/CH_3NH_3Pb(As)I_3(Cl)$ cell. Only C:N composition is calculated separately.

Additive	Pb (%)	As (%)	I (%)	Cl (%)	C:N
NH_4Cl + As	35.9	2.1	56.6	5.4	63.8:36.2

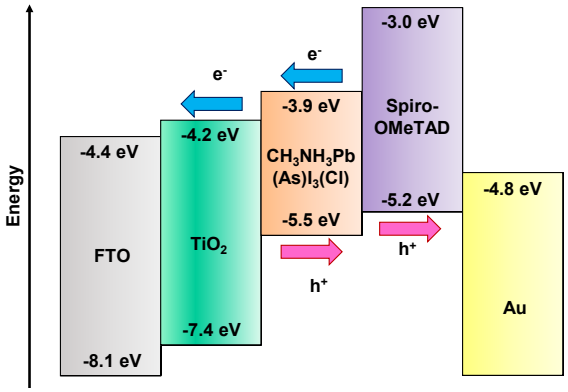

Figure 7. Energy level diagram of $CH_3NH_3Pb(As)I_3(Cl)$ cells.

Three mechanisms can be considered for the improvement of the photoconversion efficiencies [12] [13]. The first is as follows: I^- ions would be attracted at the I sites by As^{3+} with more ionic valence compared with that of Pb^{2+}, which resulted in the suppression of PbI_2 elimination from $CH_3NH_3PbI_3$. This would improve the $TiO_2/CH_3NH_3PbI_3$ interfacial structure, which improve the V_{OC} values. As the amount of arsenic increases, the lattice constants would decrease by a smaller ionic size of As^{3+} (0.76 Å) compared with that of Pb^{2+} (1.49 Å).

The second mechanism is as follows: when a small amount of Cl was doped in the $CH_3NH_3PbI_3$, diffusion length of excitons would be lengthened [9] [10], which results in the increase of the J_{SC} values.

The third is as follows: by adding AsI_3 with NH_4Cl to the $CH_3NH_3PbI_3$, the homogeneous surface and interface were formed, which improved the photovoltaic properties, especially the *FF* values. In addition, the doping effects of As and Cl would also contribute the improvement of the J_{SC} values. However, further studies are needed for the photovoltaic mechanism.

4. Conclusion

$CH_3NH_3PbI_3$ perovskite solar cells co-doped with As and Cl were fabricated and characterized. Results of *J- V* characteristics and IPCE showed that the photovoltaic properties of the perovskite solar cells were improved by adding a small amount of AsI_3 and NH_4Cl to perovskite precursor solutions. XRD indicated suppression of PbI_2 formation by AsI_3 addition, and I^- ions would be attracted at the I sites by As^{3+} with more ionic valence compared with that of Pb^{2+}, which led to the suppression of PbI_2 elimination from $CH_3NH_3PbI_3$, and this would improve the $TiO_2/CH_3NH_3PbI_3$ interfacial structure. The microstructure structure analysis also indicated formation of a homogeneous microstructure by adding AsI_3 with NH_4Cl, which would improve the *FF* values. SEM-EDS analysis

showed the deficiency of iodine in the perovskite phase, which would lead to higher hole concentration and increase of J_{SC} which improved the V_{OC} values. A small amount of Cl was also doped in the $CH_3NH_3PbI_3$ from the EDS analysis, and the diffusion length of excitons would be lengthened, which resulted in the increase of the J_{SC} values. From these combining effects, the photovoltaic properties of the $CH_3NH_3Pb(As)I_3(Cl)$ cell were improved.

Acknowledgements

This work was partly supported by Satellite Cluster Program of the Japan Science and Technology Agency, and a Grant-in-Aid for Scientific Research (C) No. 25420760.

References

[1] Kojima, A., Teshima, K., Shirai, Y. and Miyasaka, T. (2009) Organometal Halide Perovskites as Visible-Light Sensitizers for Photovoltaic Cells. *Journal of the American Chemical Society*, **131**, 6050-6051. https://doi.org/10.1021/ja809598r

[2] Burschka, J., Pellet, N., Moon, S.J., Humphry-Baker, R., Gao, P., Nazeeruddin, M.K. and Grätzel, M. (2013) Sequential Deposition as a Route to High-Performance Perovskite-Sensitized Solar Cells. *Nature*, **499**, 316-320. https://doi.org/10.1038/nature12340

[3] Zhou, H., Chen, Q., Li, G., Luo, S., Song, T.B., Duan, H.S., Hong, Z., You, J., Liu, Y. and Yang, Y. (2014) Interface Engineering of Highly Efficient Perovskite Solar Cells. *Science*, **345**, 542-546. https://doi.org/10.1126/science.1254050

[4] Jeon, N.J., Noh, J.H., Yang, W.S., Kim, Y.C., Ryu, S., Seo, J. and Seok, S.I. (2015) Compositional Engineering of Perovskite Materials for High-Performance Solar Cells. *Nature*, **517**, 476-480. https://doi.org/10.1038/nature14133

[5] Saliba, M., Orlandi, S., Matsui, T., Aghazada, S., Cavazzini, M., Correa-Baena, J.P., Gao, P., Scopelliti, R., Mosconi, E., Dahmen, K.H., De Angelis, F., Abate, A., Hagfeldt, A., Pozzi, G., Graetzel, M. and Nazeeruddin, M.K. (2016) A Molecularly Engineered Hole-Transporting Material for Efficient Perovskite Solar Cells. *Nature Energy*, **1**, Article No. 15017.

[6] Nie, W., Tsai, H., Asadpour, R., Blancon, J.C., Neukirch, A.J., Gupta, G., Crochet, J. J., Chhowalla, M., Tretiak, S., Alam, M.A., Wang, H.L. and Mohite, A.D. (2015) High-Efficiency Solution-Processed Perovskite Solar Cells with Millimeter-Scale Grains. *Science*, **347**, 522-525. https://doi.org/10.1126/science.aaa0472

[7] Shi, D., Adinolfi, V., Comin, R., Yuan, M., Alarousu, E., Buin, A., Chen, Y., Hoogland, S., Rothenberger, A., Katsiev, K., Losovyj, Y., Zhang, X., Dowben, P.A., Mohammed, O.F., Sargent, E.H. and Bakr, O.M. (2015) Low Trap-State Density and Long Carrier Diffusion in Organolead Trihalide Perovskite Single Crystals. *Science*, **347**, 519-522. https://doi.org/10.1126/science.aaa2725

[8] Oku, T., Suzuki, K. and Suzuki, A. (2016) Effects of Chlorine Addition to Perovskite-Type $CH_3NH_3PbI_3$ Photovoltaic Devices. *Journal of the Ceramic Society of Japan*, **124**, 234-238. https://doi.org/10.2109/jcersj2.15250

[9] Stranks, S.D., Eperon, G.E., Grancini, G., Menelaou, C., Alcocer, M.J.P., Leijtens, T., Herz, L.M., Petrozza, A. and Snaith, H.J. (2013) Electron-Hole Diffusion Lengths Exceeding 1 Micrometer in an Organometal Trihalide Perovskite Absorber. *Science*, **342**, 341-344. https://doi.org/10.1126/science.1243982

[10] Dong, Q., Fang, Y., Shao, Y., Mulligan, P., Qiu, J., Cao, L. and Huang, J. (2015)

Electron-Hole Diffusion Lengths > 175 μm in Solution-Grown $CH_3NH_3PbI_3$ Single Crystals. *Science*, **347**, 967-970. https://doi.org/10.1126/science.aaa5760

[11] Hao, F., Stoumpos, C.C., Cao, D.H., Chang, R.P. and Kanatzidis, M.G. (2014) Lead-Free Solid-State Organic-Inorganic Halide Perovskite Solar Cells. *Nature Photonics*, **8**, 489-494. https://doi.org/10.1038/nphoton.2014.82

[12] Oku, T., Ohishi, Y. and Suzuki, A. (2016) Effects of Antimony Addition to Perovskite-Type $CH_3NH_3PbI_3$ Photovoltaic Devices. *Chemistry Letters*, **45**, 134-136. https://doi.org/10.1246/cl.150984

[13] Oku, T., Ohishi, Y., Suzuki, A. and Miyazawa, Y. (2016) Effects of Cl Addition to Sb-Doped Perovskite-Type $CH_3NH_3PbI_3$ Photovoltaic Devices. *Metals*, **6**, 147.

[14] Krishnamoorthy, T., Ding, H., Yan, C., Leong, W.L., Baikie, T., Zhang, Z., Sherburne, M., Li, S., Asta, M., Mathews, N. and Mhaisalkar, S.G. (2015) Lead-Free Germanium Iodide Perovskite Materials for Photovoltaic Applications. *Journal of Materials Chemistry A*, **3**, 23829-23832. https://doi.org/10.1039/C5TA05741H

[15] Ohishi, Y., Oku, T. and Suzuki, A. (2016) Fabrication and Characterization of Perovskite-Based $CH_3NH_3Pb_{1-x}Ge_xI_3$, $CH_3NH_3Pb_{1-x}Tl_xI_3$ and $CH_3NH_3Pb_{1-x}In_xI_3$ Photovoltaic Devices. *AIP Conference Proceedings*, **1709**, Article ID: 020020.

[16] Zuo, C. and Ding, L. (2014) An 80.11% FF Record Achieved for Perovskite Solar Cells by Using the NH_4Cl Additive. *Nanoscale*, **6**, 9935-9938. https://doi.org/10.1039/C4NR02425G

[17] He, J. and Chen, T. (2015) Additive Regulated Crystallization and Film Formation of $CH_3NH_3PbI_{3-x}Br_x$ for Highly Efficient Planar-Heterojunction Solar Cells. *Journal of Materials Chemistry A*, **3**, 18514-18520. https://doi.org/10.1039/C5TA05373K

[18] Kim, H.B., Choi, H., Jeong, J., Kim, S., Walker, B., Song, S. and Kim, J.Y. (2014) Mixed Solvents for the Optimization of Morphology in Solution-Processed, Inverted-Type Perovskite/Fullerene Hybrid Solar Cells. *Nanoscale*, **6**, 6679-6683. https://doi.org/10.1039/c4nr00130c

[19] Oku, T., Zushi, M., Imanishi, Y., Suzuki, A. and Suzuki, K. (2014) Microstructures and Photovoltaic Properties of Perovskite-Type $CH_3NH_3PbI_3$ Compounds. *Applied Physics Express*, **7**, Article ID: 121601. https://doi.org/10.7567/APEX.7.121601

[20] Wyckoff, R.W.G. (1963) Second Edition. Interscience Publishers, New York Note: Cadmium Iodide Structure. *Crystal Structure*, **1**, 239-444.

[21] Hom, M., Schwerdtfeger, C.F. and Meagher, E.P. (1977) Refinement of the Structure of Anatase at Several Temperatures. *Zeitschrift fuer Kristallographie*, *Kristallgeometrie*, *Kristallphysik*, *Kristallchemie*, **136**, 273-281.

[22] Baur, W.H. and Khan, A.A. (1971) Rutile-Type Compounds.VI.SiO_2, GaO_2 and a Comparison with Other Rutile-Type Structure. *Acta Crystallographica*, **B27**, 2133-2139. https://doi.org/10.1107/S0567740871005466

[23] Oku, T. (2015) Crystal Structures of $CH_3NH_3PbI_3$ and Related Perovskite Compounds Used for Solar Cells. In: Kosyachenko, L.A., Ed., *Solar Cells—New Approaches and Reviews*, InTech, Rijeka, 77-102.